NASA Technical Memorandum 86658

USAAVSCOM TM 84-A-10

NASA-TM-86658

19850012803

Transonic Interaction of Unsteady Vortical Flows

W.J. McCroskey and G.R. Srinivasan

December 1984

National Aeronautics and Space Administration

NF00638

United States Army Aviation Systems Command

NASA Technical Memorandum 86658 USAAVSCOM TM 84-A-10

Transonic Interaction of Unsteady Vortical Flows

W. J. McCroskey, Aeromechanics Laboratory, U. S. Army Research & Technology Laboratories-AVSCOM, Ames Research Center, Moffett Field, California
G. R. Srinivasan, JAI Associates, Mountain View, California

National Aeronautics and Space Administration
Ames Research Center
Moffett Field. California 94035

United States Army
Aviation Systems
Command
St. Louis, Missouri 63120

TRANSONIC INTERACTIONS OF UNSTEADY VORTICAL FLOWS

W. J. McCroskey*
U.S. Army Aeromechanics Laboratory (AVSCOM)
NASA Ames Research Center, Moffett Field, California

G. R. Srinivasan†
JAI Associates, Mountain View, California

Abstract

Unsteady interactions of strong concentrated vortices, distributed gusts, and sharp-edged gusts with stationary airfoils have been analyzed in two-dimensional transonic flow. A simple and efficient method for introducing such vortical disturbances has been implemented in numerical codes that range from inviscid transonic small-disturbance to thin-layer Navier Stokes. The numerical results demonstrate the large distortions in the overall flow field and in the surface air loads that are produced by various vortical interactions. The results of the different codes are in excellent qualitative agreement, but, as might be expected, the transonic small-disturbance calculations are deficient in the important region near the leading edge.

Introduction

Vortical disturbances can have important effects on the airloads and the aeroacoustics of a variety of aerodynamic devices, such as maneuvering aircraft and missiles, helicopter rotor blades, and turbomachinery. Although the numerical analysis of strong vortical flows has received less attention than the treatment of shock waves over the past decade, compressible flow fields with embedded regions of distributed or concentrated vorticity appear certain to receive increasing attention in the future.

Several methods have already begun to appear in the literature for treating concentrated vorticity in finite-difference computations. Direct approaches, such as Rizzi and Erickson,[1] Fujii and Kutler,[2] Krause,[3] and Srinivasan and Steger[4] may be classified as vortex-capturing, by analogy with the familiar shock-capturing methods that are used in many computational fluid dynamics (CFD) codes. As in shock capturing, the details of the actual phenomenon are spread over several grid points. Consequently, the solutions in these high-gradient regions are artificially grid-dependent and are susceptible to the effects of numerical dissipation. In the case of concentrated-tip vortices, for example, numerical dissipation may destroy the simulation of the core structure faster than would physical dissipation,[4] unless many grid points are clustered in the vortical region.

Two alternate methods for modeling vortex flows are illustrated schematically in Fig. 1. By analogy with shock-fitting in transonic flows, these methods may be thought of as vortex-fitting. The upper part of the figure portrays the method introduced by Caradonna et al.,[5] and used by George and Chang,[6] for example. This technique of one or more branch cuts permits concentrated vortices to be introduced into potential-flow formulations.

The prescribed-vortex method, which is the subject of this paper, is shown in the lower half of Fig. 1. The essential ideas are due to Steinhoff[7] and Buning and Steger,[8] and the technique has been used by the authors[9-11] for potential, Euler, and thin-layer Navier-Stokes analyses of two-dimensional, unsteady airfoil-vortex interactions. In these applications, the structure of the vortex is prescribed, but its path in space can be allowed to develop as part of the solution. The prescribed-disturbance method is also well suited to and has been used for more general vortical flows, such as gusts with distributed vorticity.[12]

Many of the interesting practical applications, such as blade-vortex interactions of helicopter rotors (e.g., Fig. 2), and gust response of aircraft wings, are three-dimensional unsteady problems that will require enormous computational resources for transonic cases. Therefore, it is useful to study the numerical methods, as well as the general nature of the phenomena, in two dimensions, as indicated in the figure. It is also important to establish the minimum level of complexity in the governing equations that will suffice. In the following sections, we review our transonic small-disturbance, Euler, and thin-layer Navier-Stokes analyses, especially the two-dimensional implementation of the prescribed-disturbance approach. Several representative examples are given that illustrate the advantages, capabilities, and limitations of these different formulations, in anticipation of future extensions to real, three-dimensional problems.

---

*Senior Staff Scientist.
†Senior Research Engineer.

Presented at Symposium on Numerical and Physical Aspects of Aerodynamic Flows, Long Beach California, Jan. 14-17, 1985.

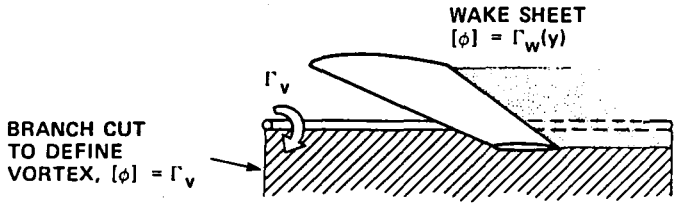

(a) POTENTIAL – FLOW VORTEX FITTING

$$\vec{q} = \vec{U}_\infty + \vec{q}_v + \Delta\vec{q}_w$$

$$d\vec{q}_v = \frac{\Gamma}{4\pi} \frac{\cos\beta\, ds}{r^2}$$

$\vec{r}_v$ CALCULATED (FORCE-FREE PATH)

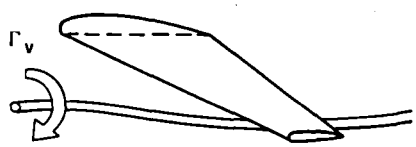

(b) PRESCRIBED – DISTURBANCE VORTEX FITTING

Fig. 1 Methods for modeling vortex flows.

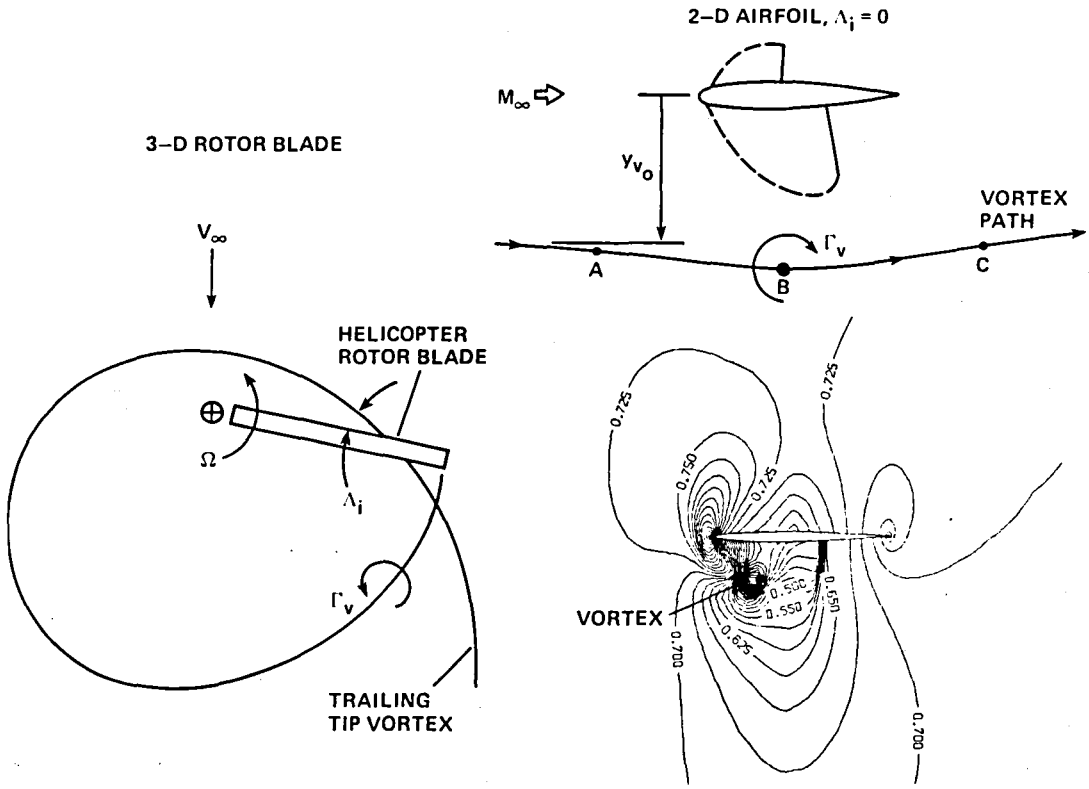

Fig. 2 Two- and three-dimensional unsteady vortex interactions.

Numerical Formulations

The essence of the prescribed-disturbance[7] or perturbation[8] method is simply that each of the dependent flow variables is split into a prescribed part, which defines (or is consistent with) the imposed vortical disturbance, and a remaining part, which is obtained from the solution of the governing equation set. Even though the governing equation(s) may be nonlinear and independent solutions are therefore not superposable, we may still decompose the dependent variables as follows:

$$q = q_v + (q - q_v) \tag{1}$$

where

$$q = \begin{bmatrix} \rho \\ \rho u \\ \rho v \\ e \end{bmatrix}$$

and q_v represents the specified vortical disturbance superimposed on a uniform free stream.

The following subsections summarize the development of the governing equations for $(q - q_v)$, and present the methods for solving them numerically. Although the overall concept is essentially the same for the Euler or Navier-Stokes formulations as for the transonic small-disturbance (potential) formulation, the actual derivations and solution techniques are rather different; therefore, they are treated separately. The complete details of each are given in Refs. 10 and 11 for the former, and in Refs. 9 and 12 for the latter.

Euler and Thin-Layer Navier-Stokes Equations

In this part of the investigation, we use the unsteady, two-dimensional equations in strong conservation-law form,[13] including the Baldwin-Lomax[14] algebraic eddy-viscosity model for thin-layer turbulent flows. In generalized coordinates (ξ, η, τ) and in the perturbation form of Buning and Steger,[8] the equations are

$$\partial_\tau(\hat{q} - \hat{q}_v) + \partial_\xi(\hat{E} - \hat{E}_v) + \partial_\eta(\hat{F} - \hat{F}_v) = Re^{-1}\partial_\eta \hat{S} \tag{2}$$

where the dependent flow-field vector is

$$\hat{q} = J^{-1}\begin{bmatrix} \rho \\ \rho u \\ \rho v \\ e \end{bmatrix}$$

and the flux vectors E, F, and S are given by

$$\hat{E} = J^{-1}\begin{bmatrix} \rho U \\ \rho u U + \xi_x p \\ \rho v U + \xi_y p \\ (e + p)U - \xi_t p \end{bmatrix}, \quad \hat{F} = J^{-1}\begin{bmatrix} \rho V \\ \rho u V + \eta_x p \\ \rho v V + \eta_y p \\ (e + p)V - \eta_t p \end{bmatrix} \tag{3}$$

$$\hat{S} = J^{-1}\begin{bmatrix} 0 \\ \mu(\eta_x^2 + \eta_y^2)u_\eta + (\mu/3)\eta_x(\eta_x u_\eta + \eta_y v_\eta) \\ \mu(\eta_x^2 + \eta_y^2)v_\eta + (\mu/3)\eta_y(\eta_x u_\eta + \eta_y v_\eta) \\ \kappa Pr^{-1}(\gamma - 1)^{-1}(\eta_x^2 + \eta_y^2)\partial_\eta a^2 \\ \quad + \mu(\eta_x^2 + \eta_y^2)(u^2 + v^2)_\eta/2 \\ \quad + (\mu/3)(\eta_x u + \eta_y v)(\eta_x u + \eta_y v_\eta) \end{bmatrix} \tag{4}$$

Here U and V are the contravariant velocities along the ξ and η directions, i.e.,

$$U = \xi_t + \xi_x u + \xi_y v \tag{5a}$$

$$V = \eta_t + \eta_x u + \eta_y v \tag{5b}$$

and J is the transformation Jacobian.[13]

In Eq. (2) $\hat{q}_v$ represents any prescribed nonuniformity superimposed on an otherwise uniform free stream. In the present investigation, a concentrated vortex is considered, either fixed in space or moving with the flow. The velocity field of the vortex is specified as

$$v(\theta) = \frac{2\pi\Gamma_v}{|\vec{r}|}\left(1 - e^{-r^2/a^2}\right) \tag{6}$$

where Γ_v is the dimensionless vortex strength and $\vec{r}(x,t)$ is the instantaneous radial distance from the vortex center. That is, the vortex-induced field $\hat{q}_v$ is irrotational outside a viscous core of radius a. Thus the vector components ρ, (ρu), (ρv), and e are determined from the inviscid (Euler) components of Eq. (2), as discussed in Refs. 10 and 11.

The usual tangency and no-slip boundary conditions on the airfoil are applied at each instant to the total flow-field vector $\hat{q}$. Surface-conforming C-type grids are used, generated by an algebraic method,[15] with clustering near the leading and trailing edges and in the vicinity of the upper and lower surface shock waves. Typical grids for viscous calculations consist of 161 to 181 points in the surface, ξ, direction, and 52 points in the normal, η, direction, extending 6 to 10 chords in all directions. Forty-five grid points in the normal direction are generally used for the inviscid cases.

An implicit, spatially factored algorithm with Euler-implicit time-differencing[13] is used to solve Eq. (2). The scheme is first-order accurate in time and second-order accurate in space. Second-order implicit smoothing and fourth-order explicit dissipation terms are added to improve the nonlinear stability. Even so, the nondimensional time steps generally have to be restricted to values on the order of 0.005 during that portion of the interaction when the vortex is close to the airfoil. The CPU solution time on the Ames

Cray X-MP computer is approximately 2 sec/time step. The inviscid cases considered in this paper required approximately 10-15 min each, and the viscous calculations about 25-30 min CPU time, after the initial, steady solution was obtained without the vortex.

The effectiveness of the present prescribed-disturbance scheme is illustrated in Fig. 3 for one of the examples to be discussed in more detail in the section on Unsteady Vortex Interactions. The figure shows the variation in lift on the airfoil as a strong, concentrated vortex passes beneath it, with and without the special treatment outlined above. The "nonperturbation" scheme essentially represents vortex capturing; that is, the vortex structure is specified only as an initial condition, when the center of the vortex is 5 chords upstream of the leading edge. Subsequently, this initial disturbance convects through the computational domain, and the numerical dissipation associated with the finite grid spacing progressively weakens the gradients and reduces the effective vortex strength substantially. This numerical error is clearly grid-dependent; however, it is completely absent in the prescribed-disturbance solutions, which are essentially independent of the grid.

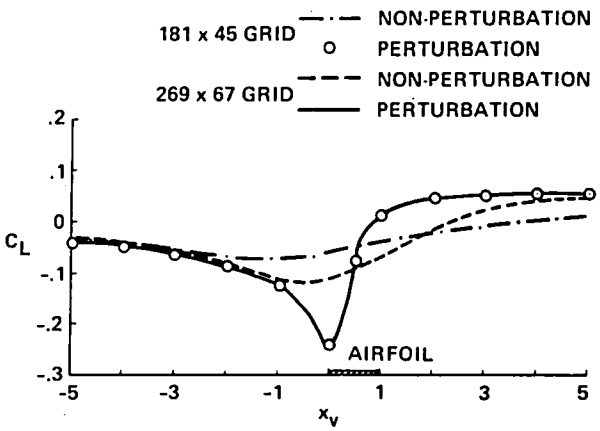

Fig. 3 Effectiveness of the prescribed-disturbance method for Euler calculations.

Transonic Small-Disturbance Potential Equation

In this case, the approximations are a thin airfoil in an inviscid, isentropic fluid, with either (1) a concentrated potential (irrotational) vortex, or (2) small distributed vortical disturbances, superimposed on an otherwise uniform, nearly sonic free stream. As in the above formulation, these prescribed vortical disturbances are assumed to not be altered by the interaction with the airfoil.

The combination of unsteady flow and rotational disturbances in the free stream requires some special attention if potential-flow concepts are to be retained. Under the previously mentioned isentropic, small-disturbance assumptions, however, the continuity and momentum equations can be combined to give[12]

$$\frac{\partial Q}{\partial t} + 2u\,\frac{\partial u}{\partial t} + (a^2 - u^2)\,\frac{\partial u}{\partial x} + a^2\,\frac{\partial v}{\partial y} = 0 \qquad (7)$$

where

$$Q = \int\left(\frac{\partial \vec{q}}{\partial t} - \vec{q} \times \nabla \times \vec{q}\right) \cdot d\vec{r} - f(t) \ , \qquad (8)$$

$d\vec{r}$ is an incremental position vector which is integrated over a suitable path from some upstream reference point, and the symbol $\vec{q}$ now represents the velocity field (u,v).

We now go a step beyond Eq. (1) and decompose this total velocity field into the following components: 1) the uniform free stream, $\vec{U}_\infty$; 2) the prescribed disturbance field, $\vec{q}_v$; and 3) an irrotational perturbation velocity field $\nabla\phi$ produced by the airfoil in the presence of the concentrated vortex or distributed gust. That is,

$$\vec{q} = \vec{U}_\infty + \vec{q}_v + \nabla\phi \qquad (9)$$

Then, for example, for a distributed vortical (rotational) gust

$$Q = \int\left(\frac{\partial \vec{q}_v}{\partial t} - \vec{q} \times \nabla \times \vec{q}_v\right) \cdot d\vec{r} + \frac{\partial \phi}{\partial t} \qquad (10a)$$

whereas for an irrotational moving vortex

$$Q = \frac{\partial \phi_v}{\partial t} + \frac{\partial \phi}{\partial t} \qquad (10b)$$

where $\phi_v = 2\pi\Gamma \tan^{-1}[(y - y_1)/(x - x_1)]$, and (x_1,y_1) is the instantaneous position of the center of the concentrated vortex.

It should be emphasized again that the decomposition of the velocity in Eqs. (1) or (9) does not imply linearity. Both the boundary conditions and the governing equation for the airfoil disturbance potential, $\nabla\phi$, are altered by the introduction of $\vec{q}_v$, and independent solutions are not superposable for transonic flows.

The governing equation for ϕ is obtained by substituting first the quantity $\vec{q}_o = \vec{U}_\infty + \vec{q}_v$, and then $\vec{q}$ given by Eq. (9), into Eq. (7). Next, the former resulting equation is subtracted from the latter. Then the quantity

$$\int\left(\frac{\partial \vec{q}_v}{\partial t} - \vec{q}_o \times \nabla \times \vec{q}_v\right) \cdot d\vec{r}$$

which is common to both, drops out. Even if $\nabla \times \vec{q}_v = 0$, the quantity $(\nabla\phi \times \nabla \times \vec{q}_v) \cdot d\vec{r}$ vanishes if $d\vec{r}$ is aligned with $\nabla\phi$. Finally, the local speed of sound, a, is evaluated using the isentropic relations and the usual tran sonic small-disturbance scaling laws and

approximations,[16-17] coupled with the observation that the prescribed disturbances considered in this paper produce only second-order variations in density, pressure, and temperature. This gives the following modified form of the unsteady transonic small-disturbance equation (in strong conservation form)

$$M_\infty^2\phi_{tt} + 2M_\infty^2\phi_{xt} = \frac{\partial}{\partial x}\left[(\beta^2 + C_2\phi_x)(\phi_x + u_v) - \beta^2 u_v\right] + \phi_{yy} \qquad (11)$$

where

$$\beta^2 = 1 - M_\infty^2$$

$$C_2 = -\frac{1}{2}(\gamma - 1)M_\infty^2$$

Linear theory can be simulated by setting $C_2 = 0$.

The boundary condition on the airfoil is obtained by simply substituting Eq. (9) into the small-disturbance approximation to flow tangency, giving

$$\left(\frac{\partial\phi}{\partial y}\right)_b = \left(\frac{\partial}{\partial t} + U_\infty\frac{\partial}{\partial x}\right)Y_b - v_v \qquad (12)$$

As noted above, neither small-amplitude gusts nor moving concentrated potential vortices produce first-order pressure fluctuations in the free stream. Therefore, consistent with our basic assumption that the prescribed vortical disturbance remains undistorted as it passes by the airfoil, we retain the usual form for the small-disturbance pressure coefficient,

$$C_p = -2(\phi_x + \phi_t) \qquad (13)$$

Numerical experimentation revealed that the most serious deficiencies of the small-disturbance formulation are 1) a limitation on the strength of the vortex and/or its closest proximity to the airfoil, and 2) the leading-edge behavior for strong interactions with very thin airfoils. The latter can be partially overcome with an ad hoc leading-edge correction to Eq. (12); viz.

$$\left(\frac{\partial\phi}{\partial y}\right)_b = \sqrt{\frac{x}{x + r_o/2\beta}}\left[\left(\frac{\partial}{\partial t} + U_\infty\frac{\partial}{\partial x}\right)Y_b - v_v\right] \qquad (12b)$$

as discussed in Ref. 10. This treatment has been found to be very satisfactory for thin airfoils, such as the NACA 64A006 considered in the section on Unsteady Vortex Interactions. However, comparisons with Euler and full-potential solutions show that it over-corrects for moderately thick airfoils, such as the NACA 0012, and that it is completely unsatisfactory for airfoils with blunter leading edges.

Equation (11) is solved using the alternating-direction-implicit numerical algorithm of the well-exercised transonic code LTRAN2,[17] with all of the high-frequency terms included[9] and provisions added for variable time steps. A rectangular cartesian grid (113 or 186 x 97) is used, with clustering near the leading and trailing edges. The CPU solution times on the Ames Cray X-MP computer range from approximately 1 to 4 min.

Comparison of Initial Solutions

A preview of the similarities and differences in representative initial solutions, representing the steady-state solutions of airfoils in uniform free streams, Fig. 4, is helpful before considering the vortical interactions in the section on Unsteady Vortex Interactions. In this and subsequent figures, the Reynolds number is 6×10^6 for the thin-layer Navier-Stokes solution, with a turbulent boundary layer assumed for the entire airfoil. The leading-edge correction in Eq. (12b) was used for the small-disturbance calculations on the NACA 64A006 airfoil, but not for the NACA 0012. The small-disturbance deficiency in the leading-edge region is more evident in the results at $M_\infty = 0.3$ than at higher Mach number.

For the NACA 0012 airfoil at $M_\infty = 0.8$, the shock wave is fairly strong, but viscous effects are relatively weak. Therefore, the Navier-Stokes and Euler solutions are approximately the same, but the details near the shock wave are slightly different in the small-disturbance solution. On the other hand, the viscous effects are stronger on the 64A006 airfoil, but the Euler and small-disturbance are almost identical. The experimental results are from Zwaan.[18]

Example Results--Unsteady Vortex Interactions

For the sake of brevity, we consider only concentrated vortices convecting with the flow past symmetrical airfoils at zero angle of attack. Therefore, all the differences between the flow fields above and below the airfoils are due solely to the vortex interaction. Examples of vortices fixed in space and of airfoils at incidence are given in Refs. 9-11.

The small-disturbance results in Fig. 5 illustrate many of the essential features of transonic airfoil-vortex interactions. For this case of a vortex with clockwise circulation passing beneath the airfoil, the vortex-induced "downwash" effect first appears as an effective negative angle of attack, Figs. 5a and 5d. Unlike the linear results, however, the transonic effects are much larger on the lower surface than they are on the upper surface. Also, the actual shape of the pressure distributions, the shock-wave strengths and positions, and the time-history of the airfoil pressures are quite different, even qualitatively, from the results for airfoil oscillations, or from the results for the sinusoidal gusts considered in the section on Airfoil-Gust Interactions.

As the vortex passes beneath the airfoil, Figs. 5b and 5e, the u-component of the vortex-induced velocity field also becomes important in the nonlinear case. After the vortex passes

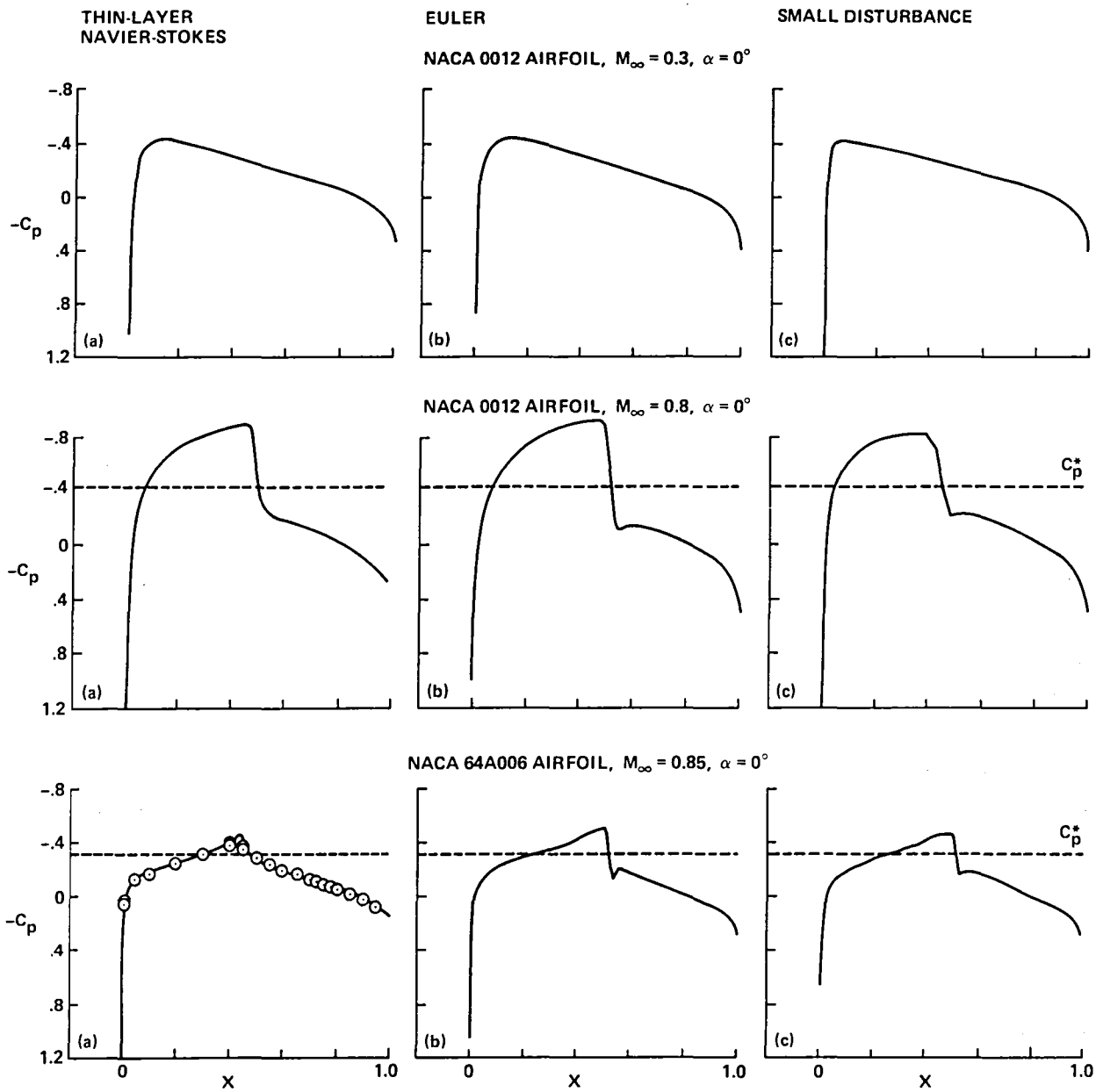

Fig. 4 Initial solutions without a vortex.

behind the trailing edge, Figs. 5c and 5f, its induced field becomes and effective "upwash" distribution of vertical velocity, and its horizontal component becomes relatively unimportant again. Throughout the interaction, nonlinear unsteady lag effects are very important, and the return of the flow around the airfoil to its orginal state is extremely slow. The moving-vortex interaction is substantially different from the quasi-steady response that would be obtained by freezing the vortex at different x-positions.

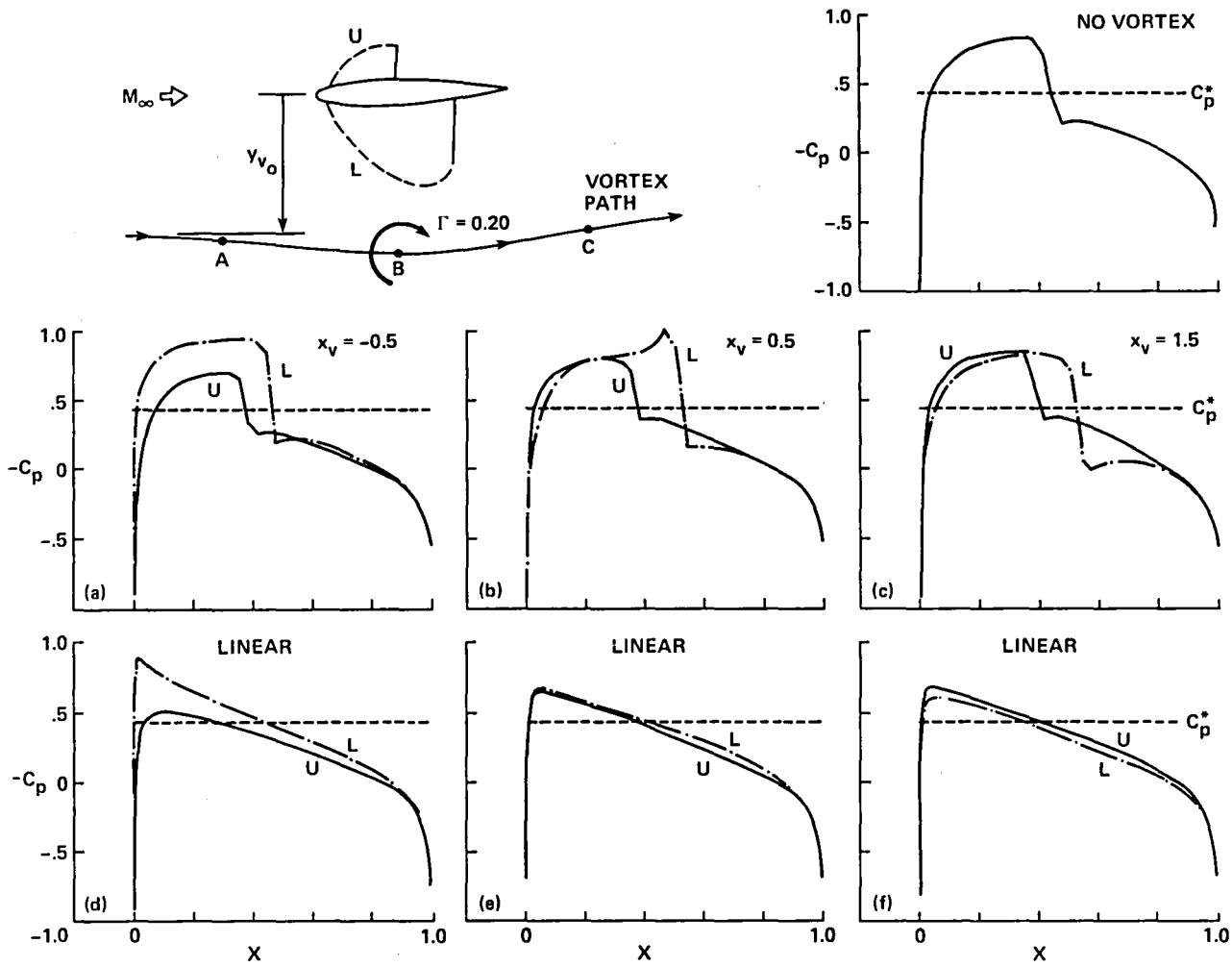

Fig. 5 Transonic airfoil-vortex interaction on the NACA 0012 airfoil at $M_\infty = 0.8$, $\alpha = 0$, $\Gamma_V = 0.20$, $y_{V_0} = -0.26$.

Figures 6 and 7 compare the transonic small-disturbance, Euler, and thin-layer Navier-Stokes results for the NACA 64A006 airfoil at $M_\infty = 0.85$, with the same vortex strength and initial position as before. This airfoil, which has been used in numerous numerical and experimental studies, is not only thinner than the NACA 0012 section, but has a significantly smaller leading-edge radius as well. Therefore, it might be expected to be more sensitive to the vortex-induced downwash than the NACA 0012 profile.

As in the steady results shown in Fig. 4, the shock wave in this case is smeared by the predicted viscous-inviscid interaction, according to the Navier-Stokes calculations. However, no boundary-layer separation is induced. Otherwise, the predictions of all three methods are similar, and the sequence of events is essentially the same as those discussed in connection with Fig. 5. However, larger fluctuations appear in the pressure distributions near the leading edge. Without the leading-edge correction of Eq. (12b) this effect was over-predicted by the small-disturbance calculations.

For the results shown in Figs. 6 and 7, the vortex is constrained to convect at U_∞ along a straight line, $y_V = -0.26$. Figure 8 shows the effect of allowing the vortex to move along a force-free path; that is, along a streamline. The Euler calculations show some differences caused by this effect as the vortex passes near and beyond the trailing edge, but this behavior is not evident in the small-disturbance results.

Instabilities usually develop in the small-disturbance calculations when cases with significantly stronger vortex interaction are attempted. The Euler and Navier-Stokes calculations require a reduction in the nondimensional time-step and require special attention to the dissipation and smoothing of parameters. However, solutions have been obtained[10,11] for values of Γ_V up to twice the values given in Figs. 5-8.

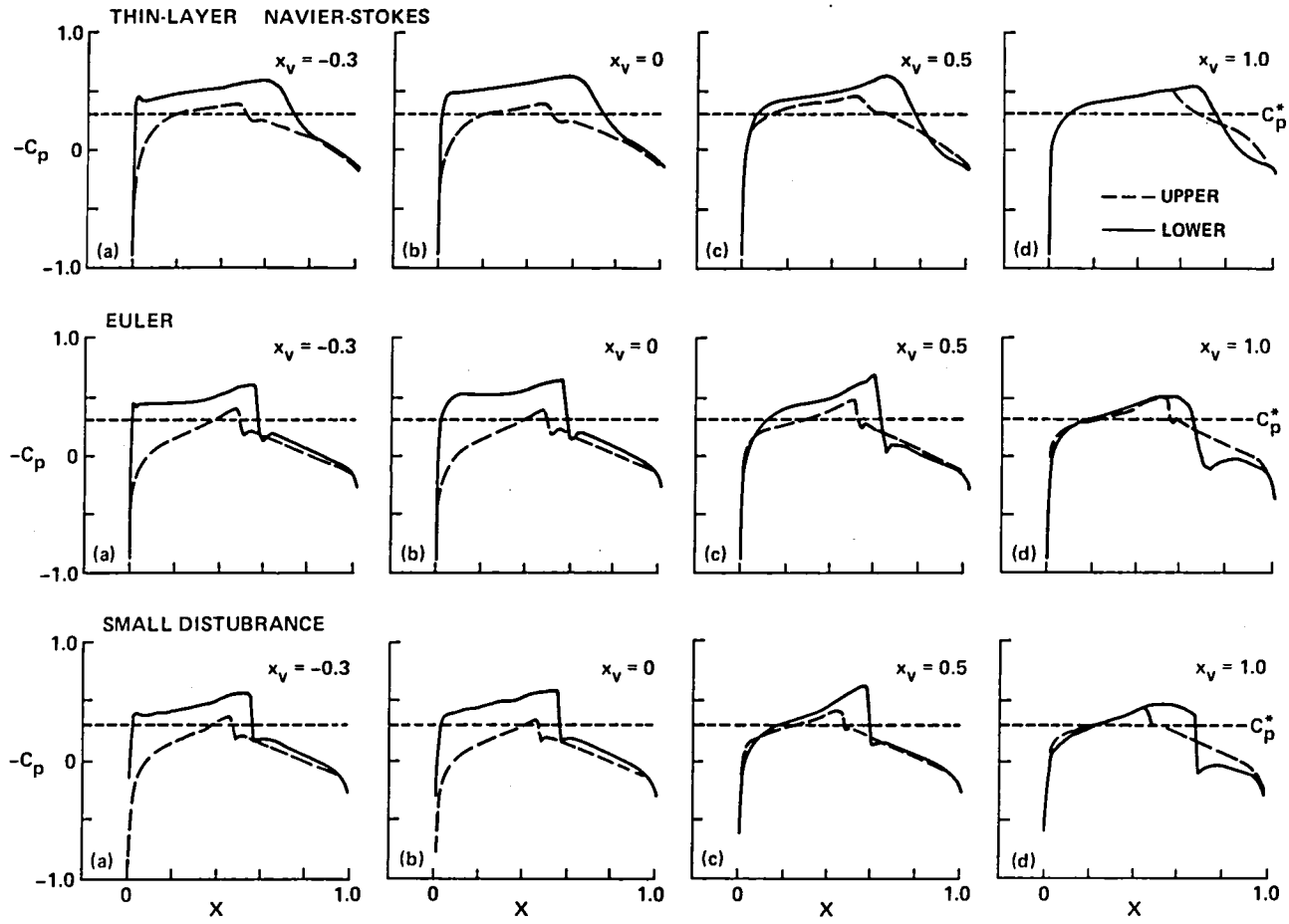

Fig. 6 Airfoil-vortex interaction on the NACA 64A006 airfoil at $M_\infty = 0.85$, $\alpha = 0$, $\Gamma_v = 0.20$, $y_v = -0.26$ = constant, Re = 6 Mil.

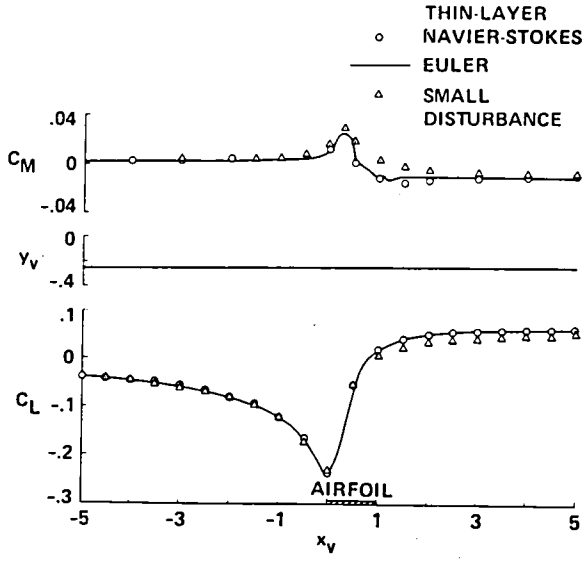

Fig. 7 Lift- and pitching-moment variations with vortex position on the NACA 64A006 airfoil at $M_\infty = 0.85$, $\alpha = 0$, $\Gamma_v = 0.20$, $y_v = -0.26$ = constant.

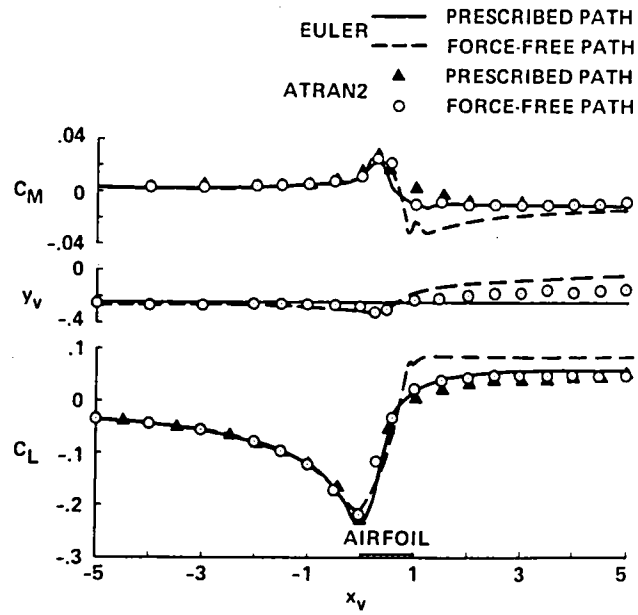

Fig. 8 Lift- and pitching-moment variations with vortex position on the NACA 64A006 airfoil at $M_\infty = 0.85$, $\alpha = 0$, $\Gamma_v = 0.20$, $y_{v_o} = -0.26$.

Examples of Airfoil-Gust Interactions

A number of calculations have been performed with the small-disturbance code for transonic flows with sinusoidal and sharp-edged gusts, whose distributions of vorticity are small in amplitude, but which are not necessarily irrotational.[12] These correspond to examples that have previously appeared in the literature for incompressible or subsonic flows.

Sinusoidal Transverse Gusts

The first case to be considered is the transonic counterpart of the well-known sinusoidal traveling-wave gust with a transverse velocity

$$v_G = A_1 \sin(\omega t - \omega\tilde{x}) \qquad (14)$$

where $\tilde{x}/c = 2x/c - 1$ is measured from the mid-chord of the airfoil, and where c is the chord. This case is particularly straightforward within the framework of the transonic small-disturbance approximation, since the gust velocity does not appear explicitly in the governing equation. The effect of the gust is felt through the boundary condition on the airfoil as an effective time- and space-dependent angle of attack, Eq. (12).

A sketch of this problem and typical results for this type of gust are shown in Fig. 9; the figure shows computations for both the nonlinear and linear mode of Eq. (11) at various "phases" during the passage of the gust. This figure may be compared with Fig. 5, for which the airfoil, Mach number, and mean angle of attack are the same. Here the nondimensional frequency parameter, $K = \omega c/U_\infty$, is inversely proportional to the wave length λ of the gust; $\lambda = 2\pi U_\infty/\omega = 4\pi c$ in this particular case. The amplitude of the gust corresponds to an effective fluctuating angle of attack of ±1°.

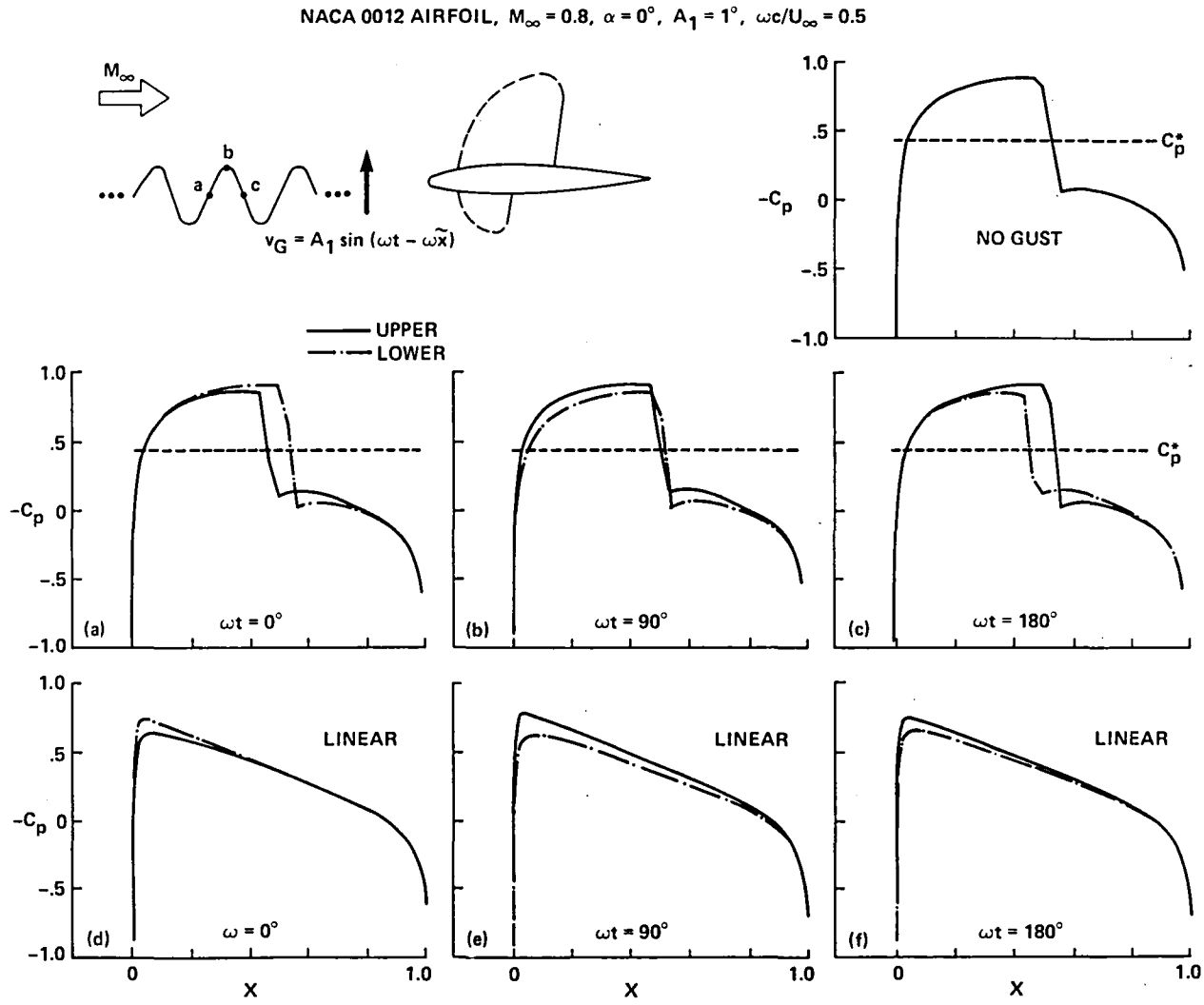

Fig. 9 Transonic airfoil-gust interaction on the NACA 0012 airfoil at $M_\infty = 0.8$, $\alpha = 0$; sinusoidal gust with $A_1 = 0.017$, $\omega c/U_\infty = 0.5$.

The main distinction of the linear and nonlinear solutions in Fig. 9 is the presence of a shock wave and its unsteady motion as the gust passes by the airfoil. The role of moving shock waves is even more dramatic in the following example, which is a comparison of the conventional NACA 0012 airfoil and a modern supercritical profile.

Computed results for the Dornier CAST-7 and NACA 0012 airfoils with significant amounts of lift are compared in Figs. 10 and 11. Figure 11 shows the harmonic components of the surface pressure distributions, referenced to the phase and amplitude of the prescribed gust. The nonlinear effects are much stronger on the upper surface than in the previous example. It is interesting to note that upper-surface shock wave is much stronger on the NACA 0012 than on the CAST-7 airfoil, with correspondingly larger magnitudes of pressure fluctuations in the neighborhood of a shock wave. However, the shock-wave motion is much greater on the CAST-7 airfoil, to the extent that the mean C_p distribution in Fig. 11 is significantly different from the C_p distribution without the gust, Fig. 10.

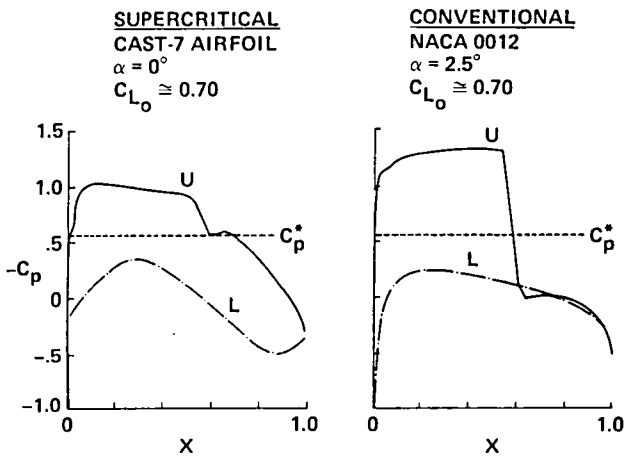

Fig. 10 Steady Transonic flow on supercritical and conventional airfoils at $M_\infty = 0.76$.

The lower surfaces of both airfoils remain subcritical throughout most of the cycle of the gust interaction. Consequently, both curves of mean C_p in Fig. 11 are approximately equivalent to the respective lower-surface steady values in Fig. 10 and there is no higher-harmonic content. There are only mild distortions of the first-harmonic fluctuating pressures in the vicinity of the shock wave, and the overall features approximately resemble the linear solutions (not shown).

Sharp-Edged Gusts--Indicial Response

Indicial responses to impulsive plunging motion, step changes in angle of attack, and sharp-edged gusts are often used in linear analyses to determine the aerodynamic loads for arbitrary body motions or gust fields. Ballhaus and Goorjian[19] have discussed how this approach can be extended to a limited class of transonic

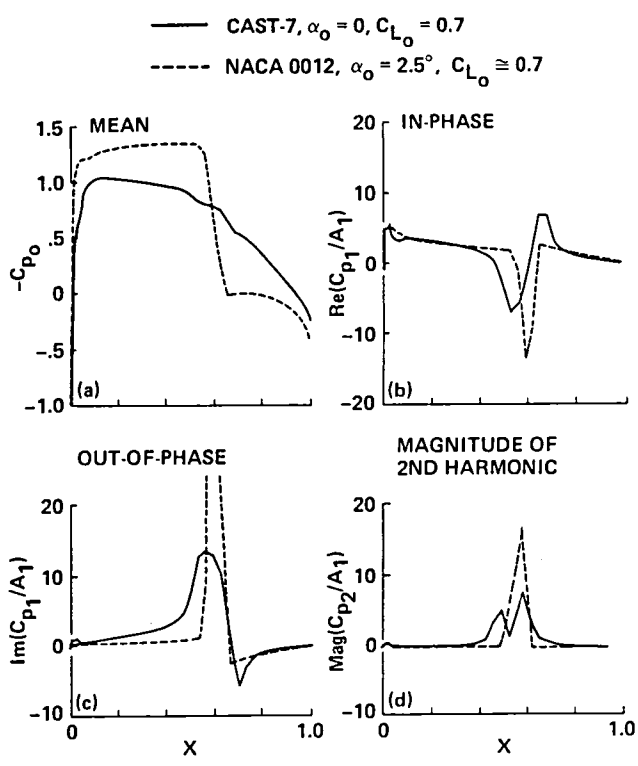

(a) Upper surface.

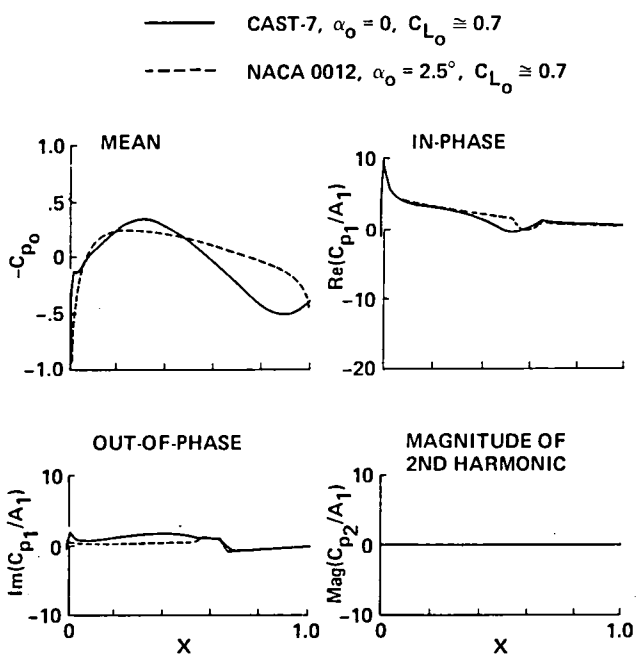

(b) Lower surface.

Fig. 11 Harmonic components of the pressure distributions on supercritical and conventional airfoils at $M = 0.76$; sinusoidal gust with $A_1 = 0.017$, $\omega c/U_\infty = 0.5$.

oscillating airfoil problems, if the shock-wave motion is negligible and the unsteady fluctuations are essentially linear perturbations about a nonlinear steady or mean flow. In this section we

discuss the indicial response to a sharp-edged gust, Fig. 12, in subsonic and transonic flow.

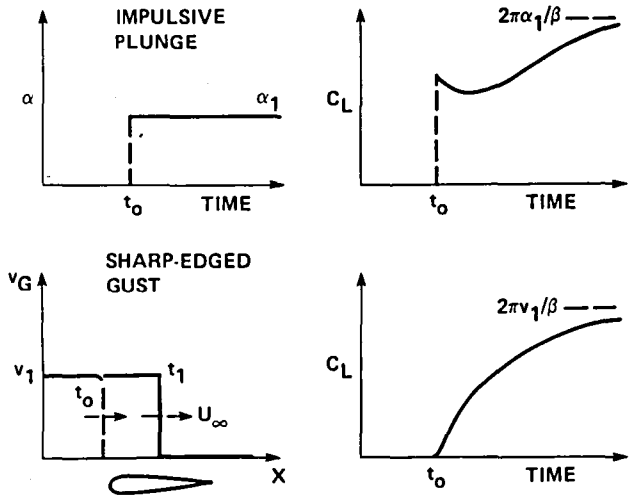

Fig. 12 Schematic of indicial response for plunging motion (above) and for a sharp-edged gust (below).

Figure 12 illustrates the similarities and differences in the response of a thin airfoil to two types of indicial inputs; namely,

$$\text{plunge:} \quad \alpha = \begin{cases} 0 & \text{for} \quad t < 0 \\ A_1 & \text{for} \quad t > 0 \end{cases} \tag{15}$$

$$\text{gust:} \quad v_G = \begin{cases} 0 & \text{for} \quad U_\infty t < X \\ A_1 & \text{for} \quad U_\infty t > X \end{cases} \tag{16}$$

According to linear theory,[20] the sharp-edged gust response rises monotonically from zero at $t = 0$ to the value $C_L = 2\pi A_1/(1 - M_\infty^2)^{1/2}$ as $t \to \infty$, whereas the plunge response starts at $C_L = \pi A_1$ for $M_\infty = 0$ and at $4A_1/M_\infty$ for $M_\infty > 0$. In either case, the approach to the steady-state value is progressively slower as M_∞ increases.

Figure 13 shows the nonlinear gust response of the NACA 64A006 airfoil as a function of Mach number, with a logarithmic abscissa. The critical Mach number for this airfoil is approximately 0.83 for $\alpha = 0$, and the flow is only weakly transonic at $M_\infty = 0.80$ and $\alpha = 1°$. Therefore, the lift response shown in Fig. 13 is essentially linear for $M_\infty \leq 0.80$.

However, the behavior becomes distinctly nonlinear at higher Mach numbers. The overshoot in lift at $M_\infty = 0.9$ is due to a complex, nonlinear motion of the shock wave on the lower surface, as shown in Fig. 14. The upper-surface shock wave moves monotonically rearward from its initial position of $x = 0.85$ and stabilizes at the trailing edge at $U_\infty t/c = 25$. However, the shock wave on the lower surface moves forward initially, reaches a minimum value of X_s at $U_\infty t/c = 30$, and then undergoes a small oscillation in position between $U_\infty t/c = 40$ and 60, before reaching its final rearward location. This nonlinear behavior indicates that it would be a mistake to use the indicial gust response at $M_\infty = 0.9$ in a superposition integral for arbitrary wave forms.

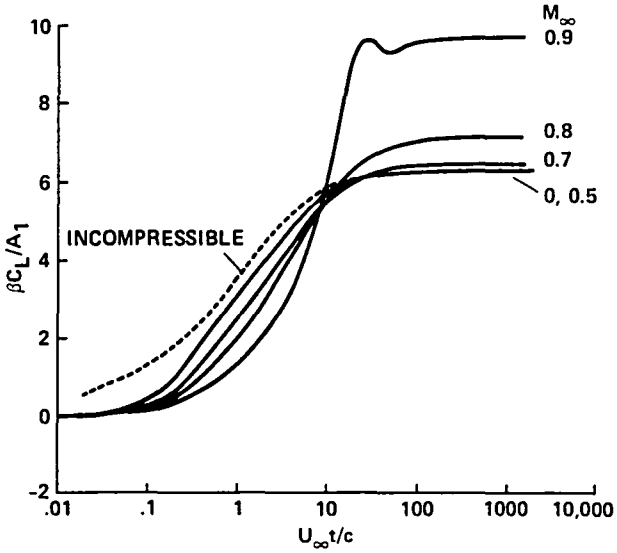

Fig. 13 Indicial gust response on the NACA 64A0012 airfoil.

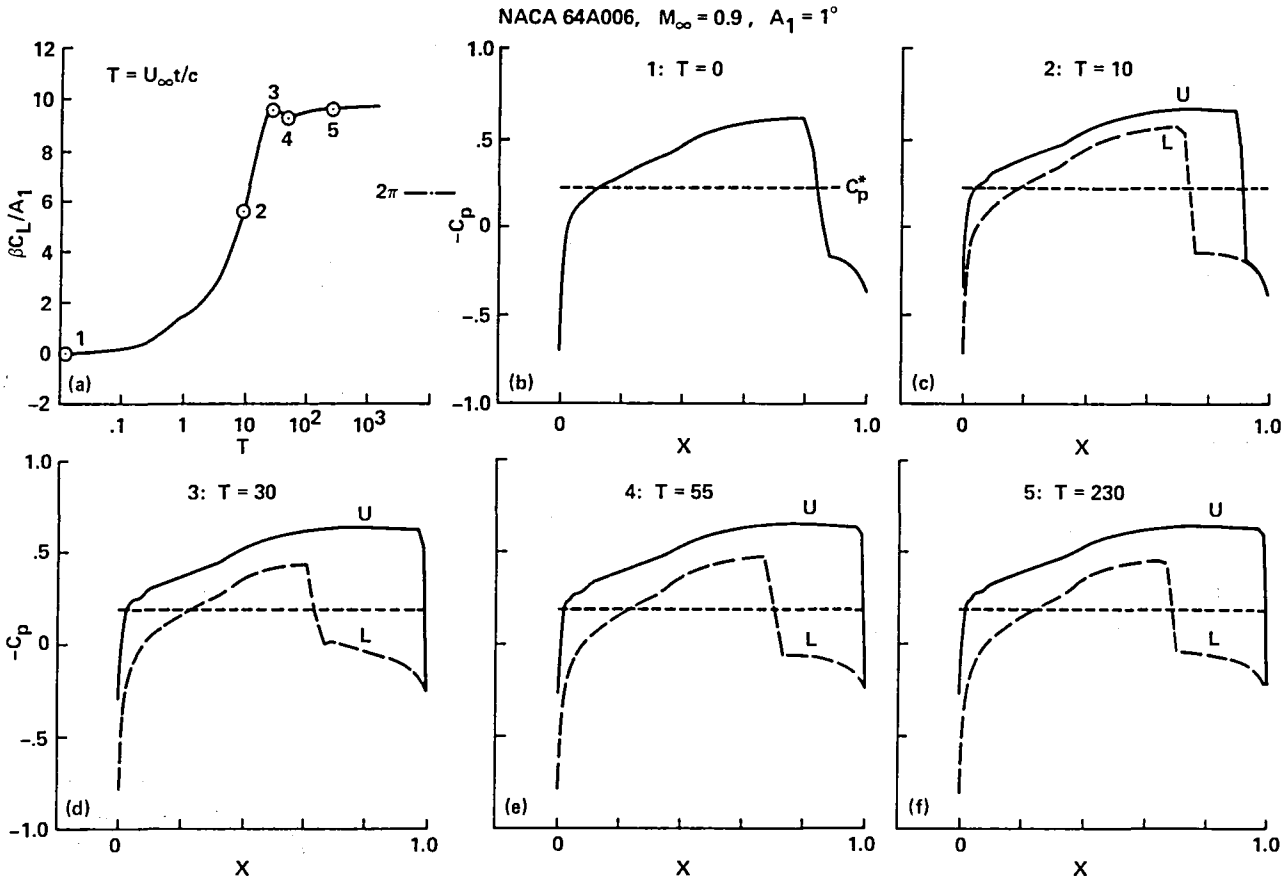

Fig. 14 Nonlinear indicial gust response and instantaneous pressure distributions on the NACA 64A0012 airfoil at $M_\infty = 0.9$ and $A_1 = 0.017$.

Summary and Conclusions

The prescribed-disturbance method has proven to be a simple and efficient method for introducing vortical disturbances into numerical codes for transonic flow analyses, including inviscid transonic small-disturbance, Euler, and thin-layer Navier-Stokes formulations. The technique has permitted the interaction of strong concentrated vortices, small-amplitude distributed gusts, and sharp-edged gusts with stationary lifting surfaces to be simulated in two-dimensional transonic flow. The results of the different codes are in excellent qualitative agreement. However, as might be expected, the transonic small-disturbance calculations can be deficient and misleading in the important region near the leading edge, unless special precautions are taken. Also, the small-disturbance code is less robust in coping with very strong vortices and with vortex paths that pass extremely close to the airfoil.

Several important features of the interaction of a concentrated vortex with an airfoil have been established. Detailed examinations of results show that the effect of the vortex is felt primarily through the vertical velocity that it induces, which to first order appears as a time-dependent perturbation in the effective angle of attack, and to a lesser extent through its horizontal induced velocity. Also, unsteady lag effects appear to be very important, especially in the transonic case. Calculations show great differences between quasi-steady and unsteady solutions and between the results for the vortex locations upstream and downstream of the airfoil. Finally, other strong nonlinear effects have been noted at transonic speeds. Even the qualitative pressure variations with respect to time and space differ markedly from the predictions of linear theory, and the vortex distorts the flow on the nearest surface of the body much more than the flow on the opposite surface.

A vortex with an assumed, invariant structure has been considered thus far. In reality, close encounters with a body will probably alter the vortex core significantly and may lead to vortex bursting; this aspect of the problem needs to be examined. For most practical applications, including helicopter rotors, future studies need to be extended to include three dimensions, where it will be even more essential to minimize the level of complexity in the governing equations without sacrificing accuracy.

The transonic small-disturbance formulation has been extended to include distributed vortical

disturbances superimposed on a uniform free stream, under the assumption that the prescribed disturbance remains undistorted as it convects past a thin airfoil. A number of unsteady airfoil-gust interactions have been calculated within this framework, and sample results illustrate the essential effects of periodic gusts on the transonic flow around conventional and supercritical airfoils. Also, several examples of sharp-edged gusts have been studied. As in the concentrated-vortex interactions, the strength and unsteady motion of the shock wave were found to play major roles in the flow-field development and, consequently, in the airloads on the airfoil.

References

[1]Rizzi, A., Eriksson, L.-E., Schmidt, W., and Hitzel, S., "Numerical Solutions of the Euler Equations Simulating Vortex Flows Around Wings," Paper No. 21, Aerodynamics of Vortical Type Flows in Three Dimensions, AGARD CP-342, June 1983.

[2]Fujii, K. and Kutler, P., "Numerical Simulation of the Viscous Flow over Three-Dimensional Complicated Geometries," AIAA Paper 84-1550, June 1984.

[3]Krause, E., Shi, X.-G., and Hartwich, P. M., "Computation of Leading Edge Vortices," AIAA Paper 83-1907-CP, July 1983.

[4]Srinivasan, G. R. and Steger, J. L., "Computation of Wing-Vortex Interaction in Transonic Flow Using Implicit Finite Difference Algorithm," NASA CR-166251, Mar. 1981; also AIAA Paper 81-1206, June 1981.

[5]Caradonna, F. X., Tung, C., and Desopper, A., "Finite Difference Modeling of Rotor Flows Including Wake Effects," Journal of the American Helicopter Society, Vol. 29, Apr. 1984, pp. 26-33.

[6]George, A. R. and Chang, S. B., "Flow Field and Acoustics of Two-Dimensional Blade-Vortex Interactions, AIAA Paper 84-2309, Oct. 1984.

[7]Steinhoff, J., "The Treatment of Vortex Sheets in Compressible Potential Flow," AIAA Paper 83-1881-CP, July 1983.

[8]Buning, P. G. and Steger, J. L., "Solution of the Two-Dimensional Euler Equations with Generalized Coordinate Transformation Using Flux Vector Splitting," AIAA Paper 82-0971, June 1982.

[9]McCroskey, W. J. and Goorjian, P. M., "Interactions of Airfoils with Gusts and Concentrated Vortices in Unsteady Transonic Flow," AIAA Paper 83-1691, June 1983.

[10]Srinivasan, G. R., McCroskey, W. J., and Kutler, P., "Numerical Simulation of a Vortex with a Stationary Airfoil in Transonic Flow," AIAA Paper 84-0254, Jan. 1984.

[11]Srinivasan, G. R., "Computations of Two-Dimensional Airfoil-Vortex Interactions," NASA CR, to be published.

[12]McCroskey, W. J., "The Effects of Gusts on the Fluctuating Airloads of Airfoils in Transonic Flow," AIAA Paper 84-1580, June 1984.

[13]Steger, J. L., "Implicit Finite-Difference Simulation of Flow about Arbitrary Two-Dimensional Geometries," AIAA Journal, Vol. 16, No. 7, July 1978, pp. 679-686.

[14]Baldwin, B. S. and Lomax, H., "Thin Layer Approximation and Algebraic Model for Separated Turbulent Flows," AIAA Paper 78-257, Jan. 1978.

[15]Pulliam, T. H., Jesperson, D. C., and Childs, R. E., "An Enhanced Version of an Implicit Code for the Euler Equations," AIAA Paper 83-0344, Jan. 1983.

[16]Landahl, M. T., Unsteady Transonic Flow, Pergaman Press, New York, 1961, pp. 1-5.

[17]Ballhaus, W. F. and Goorjian, P. M., "Implicit Finite-Difference Computations of Unsteady Transonic Flows about Airfoils," AIAA Journal, Vol. 15, No. 12, Dec. 1977, pp. 1728-1735.

[18]Zwaan, R. J., "NACA 64A006, Oscillating Flap," in Compendium of Unsteady Aerodynamic Measurements, AGARD Report 702, Aug. 1982.

[19]Ballhaus, W. R. and Goorjian, P. M., "Computation of Unsteady Transonic Flows by the Indicial Method," AIAA Journal, Vol. 16, No. 2, Feb. 1978, pp. 117-124.

[20]Lomax, H., "Indicial Aerodynamics," AGARD Manual on Aeroelasticity, Vol. II, Ch. 6, Oct. 1968.

1. Report No. NASA TM 86658 and USAAVSCOM TM 84-A-10	2. Government Accession No.	3. Recipient's Catalog No.

4. Title and Subtitle	5. Report Date
TRANSONIC INTERACTIONS OF UNSTEADY VORTICAL FLOWS	December 1984
	6. Performing Organization Code

7. Author(s)	8. Performing Organization Report No.
W. J. McCroskey and G. R. Srinivasan (JAI Associates, Mountain View, Calif.)	85075
	10. Work Unit No.
9. Performing Organization Name and Address	
Aeromechanics Laboratory, U.S. Army Research and Technology Laboratories (AVSCOM), Ames Research Center, Moffett Field, Calif. 94035	11. Contract or Grant No.
	13. Type of Report and Period Covered
12. Sponsoring Agency Name and Address	Technical Memorandum
National Aeronautics and Space Administration Washington, D.C. 20546, and U.S. Army Aviation Systems Command, St. Louis, Mo. 63120	14. Sponsoring Agency Code

15. Supplementary Notes

Point of Contact: W. J. McCroskey, Ames Research Center, MS 202A-1, Moffett Field, Calif. 94035 (415) 694-6428 or FTS 464-6428

16. Abstract

Unsteady interactions of strong concentrated vortices, distributed gusts, and sharp-edged gusts with stationary airfoils have been analyzed in two-dimensional transonic flow. A simple and efficient method for introducing such vortical disturbances has been implemented in numerical codes that range from inviscid transonic small disturbance to thin-layer Navier Stokes. The numerical results demonstrate the large distortions in the overall flow field and in the surface air loads that are produced by various vortical interactions. The results of the different codes are in excellent qualitative agreement, but, as might expected, the transonic small-disturbance calculations are deficient in the important region near the leading edge.

17. Key Words (Suggested by Author(s))	18. Distribution Statement
Gusts Vortex interaction Unsteady transonic flow Computational aerodynamics	Unlimited Subject category - 02

19. Security Classif. (of this report)	20. Security Classif. (of this page)	21. No. of Pages	22. Price*
Unclassified	Unclassified	16	A02

*For sale by the National Technical Information Service, Springfield, Virginia 22161

End of Document